Geometrical determinant of nonlinear synaptic integration in human cortical pyramidal neurons

Jaeyoung Yoon[1,2,*], et al.[†]

[1] McGovern Institute for Brain Research, Massachusetts Institute of Technology, Cambridge, MA 02139, USA.
[2] Present address: F. M. Kirby Neurobiology Center, Boston Children's Hospital, & Harvard Medical School, Boston, MA 02115, USA.
[*] Correspondence: jy.yoon@tch.harvard.edu
[†] *Full author list to be determined*

Fig. 1

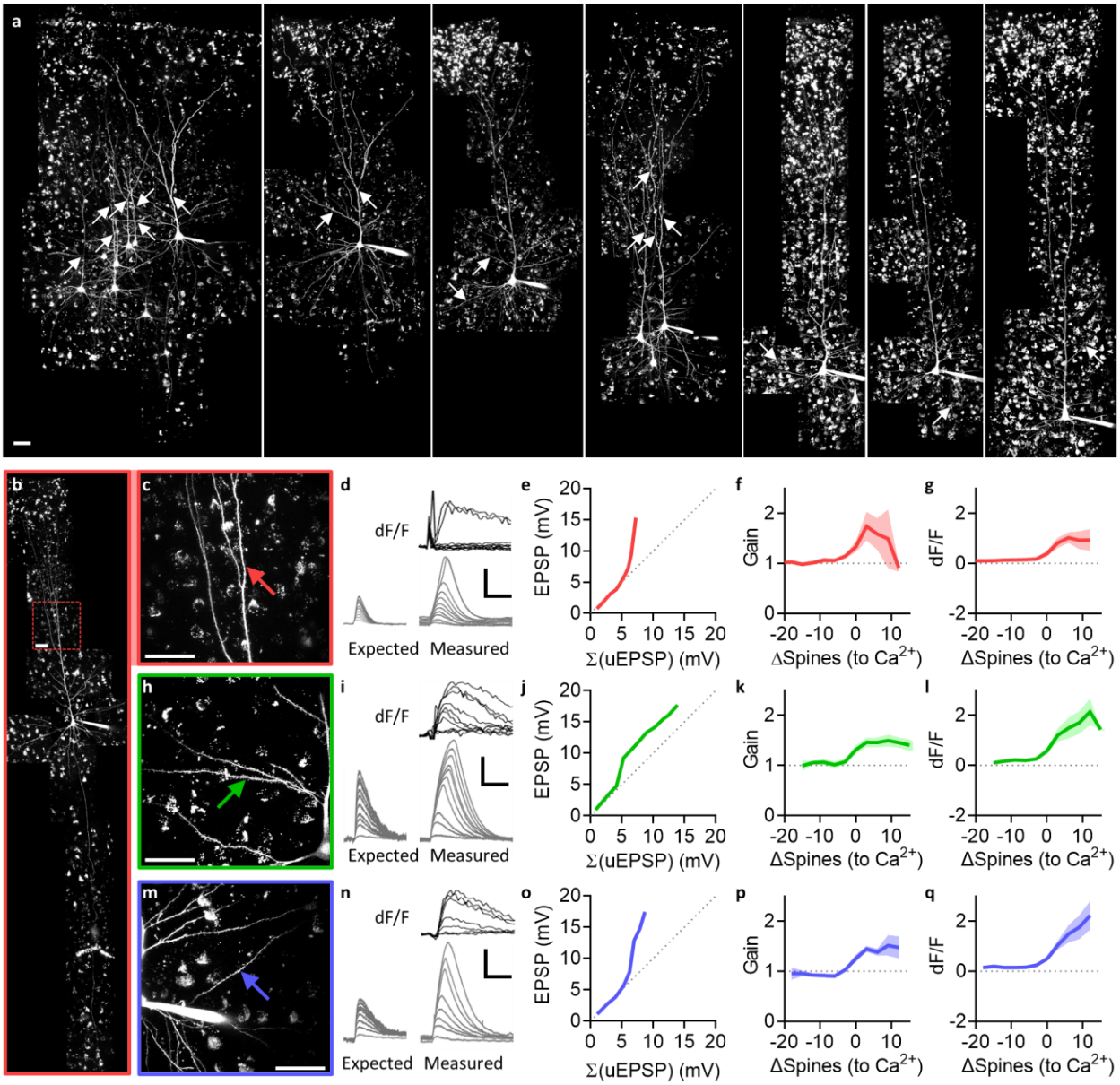
a
b
c
d
dF/F
Expected
Measured
e
EPSP (mV)
Σ(uEPSP) (mV)
f
Gain
ΔSpines (to Ca2+)
g
dF/F
ΔSpines (to Ca2+)
h
i
dF/F
Expected
Measured
j
EPSP (mV)
Σ(uEPSP) (mV)
k
Gain
ΔSpines (to Ca2+)
l
dF/F
ΔSpines (to Ca2+)
m
n
dF/F
Expected
Measured
o
EPSP (mV)
Σ(uEPSP) (mV)
p
Gain
ΔSpines (to Ca2+)
q
dF/F
ΔSpines (to Ca2+)

Figure 1. Synaptic integration at human neocortical layer 2/3 pyramidal neurons (L2/3 PN). **(a)** Representative examples of L2/3 PNs. Scale bar, 50 µm. Scale bar definitions are consistent throughout all images in all figures. Arrows indicate the center of synaptic spine clusters that were activated by 2-photon glutamate uncaging (2PGU), which typically spanned approximately 30-40 µm along the length of the branch. The high background is caused by lipofuscin aggregates on the somata of human neurons; see **Fig. 4** for comparison. **(b-c)** Representative example of an L2/3 PN, with 2PGU at the apical tuft. **(d)** Representative examples of expected EPSP (left), calculated from the arithmetic sum of unitary EPSP (uEPSP) recorded from each spine, and measured EPSP (right, bottom) recorded by quasi-simultaneous activation of spines shown in panel **c**, along with the associated fractional change in Ca^{2+} fluorescence (dF/F) obtained by intracellular calcium imaging at the parent dendrite (right, top). Scale bars, 50 ms, 5 mV, 1.0 dF/F. **(e)** Representative example of measured EPSP, plotted against the arithmetic sum of uEPSPs, from the activation of the same spines as shown in panels **b-d**. **(f)** Grouped average of synaptic gain from all apical tuft dendrites (n = 24). Gain was defined by the ratio of measured vs. expected EPSP. The number of activated spines were aligned to the threshold at which Ca^{2+} signal was first observed. **(g)** Grouped average of dF/F, associated with data shown in panel **f**. **(h-l)** Similar to panels **c-g**, but from oblique dendrites (n = 16) branching from the apical trunk. **(m-q)** Similar to panels **c-g** or **h-l**, but from basal dendrites (n = 20) branching from the soma.

Fig. 2

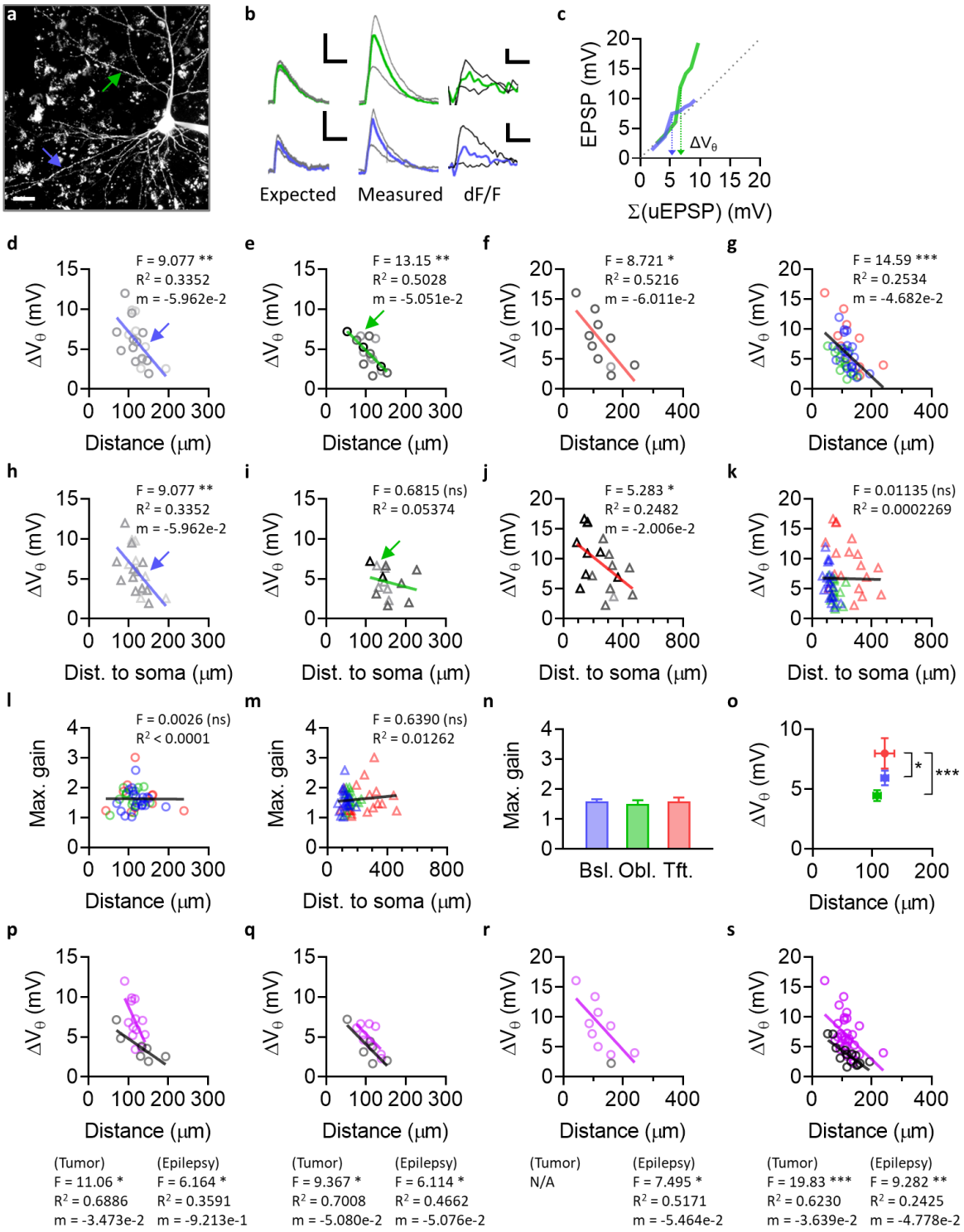
a
b
Expected
Measured
dF/F
c
EPSP (mV)
ΔVθ
Σ(uEPSP) (mV)
d
F = 9.077 **
R² = 0.3352
m = -5.962e-2
e
F = 13.15 **
R² = 0.5028
m = -5.051e-2
f
F = 8.721 *
R² = 0.5216
m = -6.011e-2
g
F = 14.59 ***
R² = 0.2534
m = -4.682e-2
ΔVθ (mV)
Distance (μm)
h
F = 9.077 **
R² = 0.3352
m = -5.962e-2
i
F = 0.6815 (ns)
R² = 0.05374
j
F = 5.283 *
R² = 0.2482
m = -2.006e-2
k
F = 0.01135 (ns)
R² = 0.0002269
Dist. to soma (μm)
l
F = 0.0026 (ns)
R² < 0.0001
m
F = 0.6390 (ns)
R² = 0.01262
n
Max. gain
Bsl. Obl. Tft.
o
*
***
p
q
r
s
(Tumor)
F = 11.06 *
R² = 0.6886
m = -3.473e-2
(Epilepsy)
F = 6.164 *
R² = 0.3591
m = -9.213e-1
(Tumor)
F = 9.367 *
R² = 0.7008
m = -5.080e-2
(Epilepsy)
F = 6.114 *
R² = 0.4662
m = -5.076e-2
(Tumor)
N/A
(Epilepsy)
F = 7.495 *
R² = 0.5171
m = -5.464e-2
(Tumor)
F = 19.83 ***
R² = 0.6230
m = -3.639e-2
(Epilepsy)
F = 9.282 **
R² = 0.2425
m = -4.778e-2

Figure 2. Somatic depolarization at nonlinearity threshold (ΔV_θ) is determined by the distance between the synapse and the nearest point on the apical trunk or the soma. **(a)** Representative example of a human L2/3 PN. Two different uncaging locations, one on a basal dendrite (blue) and another on an oblique dendrite (green), are indicated by arrows. Scale bar, 50 µm. **(b)** Representative traces of expected and measured EPSP, along with associated dF/F, from the branches shown in panel **a**. Scale bars, 50 ms, 5 mV, 0.5 (bottom) or 0.1 (top) dF/F. **(c)** Measured EPSP vs. expected EPSP from the sum of uEPSPs, from the same branches shown in panels **a-b**. **(d-g)** Somatic depolarization at nonlinearity threshold (ΔV_θ), plotted against synaptic distance. ΔV_θ was defined as the expected somatic EPSP at local nonlinearity threshold indicated by the local Ca^{2+} signal; the expected EPSP from the sum of uEPSPs was used instead of the measured EPSP to determine the correct threshold irrespective of the nonlinear gain. Synaptic distance was defined as the curvilinear projected distance along the dendrite from the synapse to the nearest point on the apical trunk or the soma. Notably, the linear regressions in panels **d-g** had similar slopes in all groups ($F = 0.06380$, $P = 0.9383$). **(d)** ΔV_θ at basal dendrites vs. distance (to soma). Shades of symbols indicate branch order (1^{st} to 4^{th}, darker to lighter, throughout panels **d-f**), which was not correlated with ΔV_θ. **(e)** ΔV_θ at oblique dendrites vs. distance (to the branch point at the apical trunk). **(f)** ΔV_θ at apical tuft dendrites vs. distance to (to the branch point at the apical trunk, i.e. nexus). **(g)** Data shown in panels **d-f**, overlaid for comparison. **(h-k)** similar to panels **d-g**, but plotted instead against distance to soma; by definition of synaptic distance used in panels **d-g**, panel **h** is identical to panel **d** (for basal dendrites only). Note that in panel **j**, synapses located at the nexus are also included, whereas they were excluded from panel **f** due to having zero synaptic distance as defined. **(l)** Maximum gain vs. synaptic distance, to the nearest point on the apical trunk or the soma. **(m)** Maximum gain vs. distance to soma. **(n)** Maximum gain at basal, oblique, and tuft dendrites. **(o)** Average ΔV_θ at basal, oblique, and tuft dendrites. **(p-s)** Same data as in panels **d-g**, but grouped separately by tumor (black) or epilepsy (purple). Neurons from the cortex associated with epilepsy had a tendency of higher ΔV_θ for a given synaptic distance, compared to those from tumor tissue.

Fig. 3

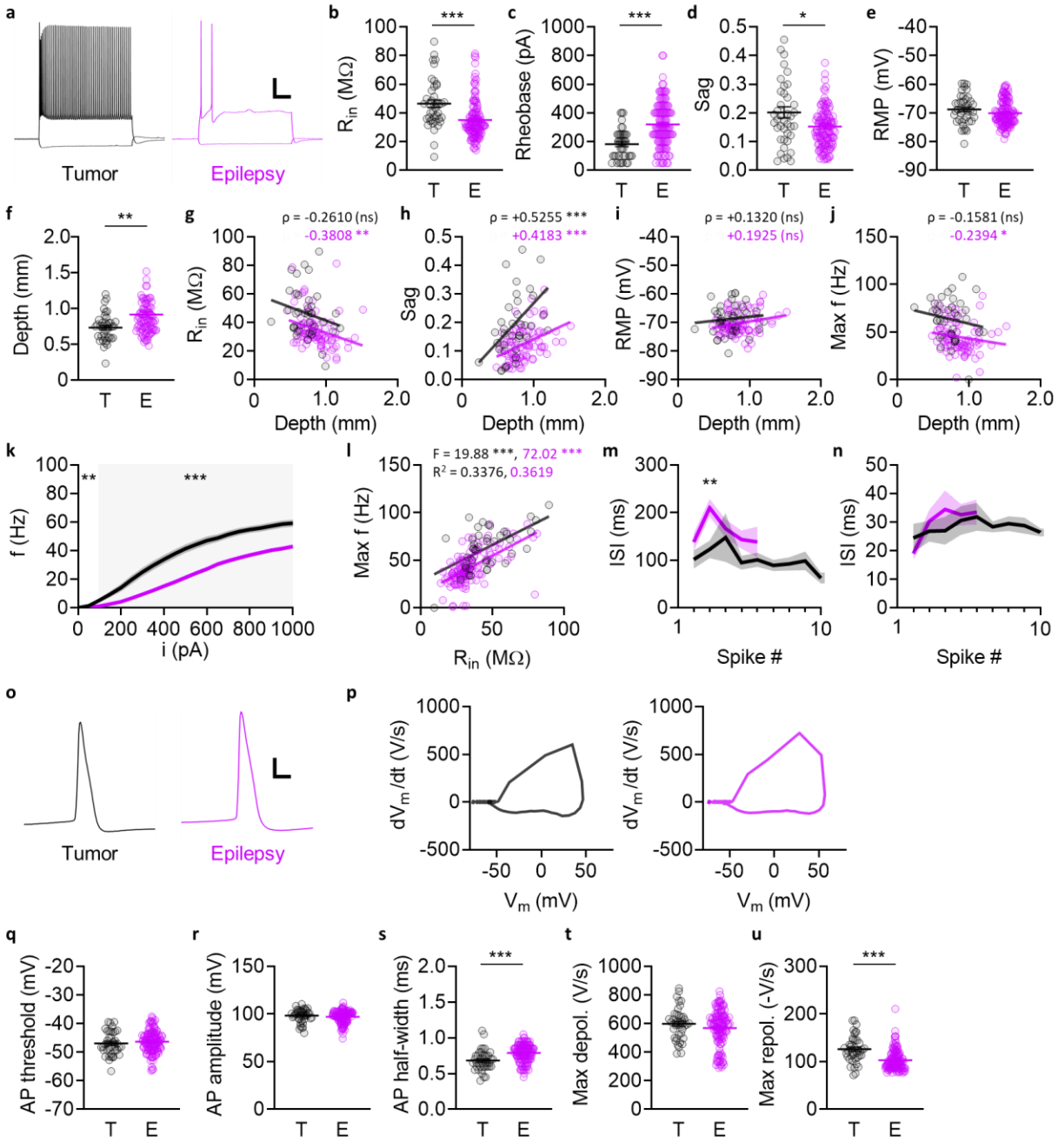
a
Tumor
Epilepsy
b
R_{in} (MΩ)
c
Rheobase (pA)
d
Sag
e
RMP (mV)
f
Depth (mm)
g
ρ = -0.2610 (ns)
-0.3808 **
h
ρ = +0.5255 ***
+0.4183 ***
i
ρ = +0.1320 (ns)
+0.1925 (ns)
j
ρ = -0.1581 (ns)
-0.2394 *
k
f (Hz)
i (pA)
l
F = 19.88 ***, 72.02 ***
R^2 = 0.3376, 0.3619
Max f (Hz)
R_{in} (MΩ)
m
ISI (ms)
Spike #
n
ISI (ms)
Spike #
o
Tumor
Epilepsy
p
dV_m/dt (V/s)
V_m (mV)
q
AP threshold (mV)
r
AP amplitude (mV)
s
AP half-width (ms)
t
Max depol. (V/s)
u
Max repol. (-V/s)

Figure 3. Intrinsic membrane properties of human L2/3 PN, from tumor (black) or epilepsy (purple). For more detailed patient and tissue information, see **Table 1**. Note that tissue from both tumor and epilepsy patients originated from areas determined to be nonpathological, but removed as part of the surgical procedure. **(a)** Representative traces of membrane potential responses to somatic step current injection (-250 pA, +1000 pA). Scale bar, 20 mV, 200 ms. The example to the right was taken from the same cell as in **Fig. 1b**. **(b)** Input resistance (R_{in}). See methods for R_{in} calculation. **(c)** Rheobase, with current step resolution of 50 pA. **(d)** Sag ratio. See methods for the definition of sag ratio. **(e)** Resting membrane potential (RMP). **(f)** Sampling bias in the cortical depths of recorded L2/3 PNs included in the current study. Cortical depth of a recorded cell was defined as the linear distance between the pial surface and the center of the mass of the somatic boundary, extrapolated from the line connecting the soma and the nexus. For all measurements of distance, the position of the soma was defined as the center of mass of its boundary. The depth of one outlier in the tumor group (235 µm) and its identity as an L2/3 PN was verified with the whole-cell 2-photon image of the cell along with neighboring L2/3 PNs deeper within the cortex, all of which had dendritic arbors that were intact up to the pia mater and in plane. **(g-j)** Intrinsic membrane properties, plotted against cortical depth. **(g)** R_{in}. **(h)** Sag ratio. **(i)** RMP. **(j)** Peak firing rate. **(k)** Firing frequency in response to somatic current injection. L2/3 PN firing frequency was significantly lower in epilepsy compared to tumor ($P < 0.001$ each for all $i \geq 100$ (pA), $P < 0.01$ for $i = 50$ (pA)). **(l)** Peak firing rate, plotted against R_{in}. **(m)** Inter-spike interval (ISI) at rheobase. **(n)** ISI at 2*rheobase. **(o)** Representative traces of single action potentials (AP) from human L2/3 PNs. For each cell, the first action potential generated at rheobase was taken for analysis. Scale bar, 20 mV, 1 ms. The example to the right was taken from the same cell as in **Fig. 2a**. **(p)** Example AP waveforms presented as dV/dt plots, calculated from the same traces as in panel **o**. **(q)** AP threshold. AP threshold was defined as the V_m at which dV/dt crossed 10 (V/s). **(r)** AP amplitude (RMP to AP peak). **(s)** AP half-width. **(t)** Maximum rate of depolarization. **(u)** Maximum rate of repolarization.

Fig. 4

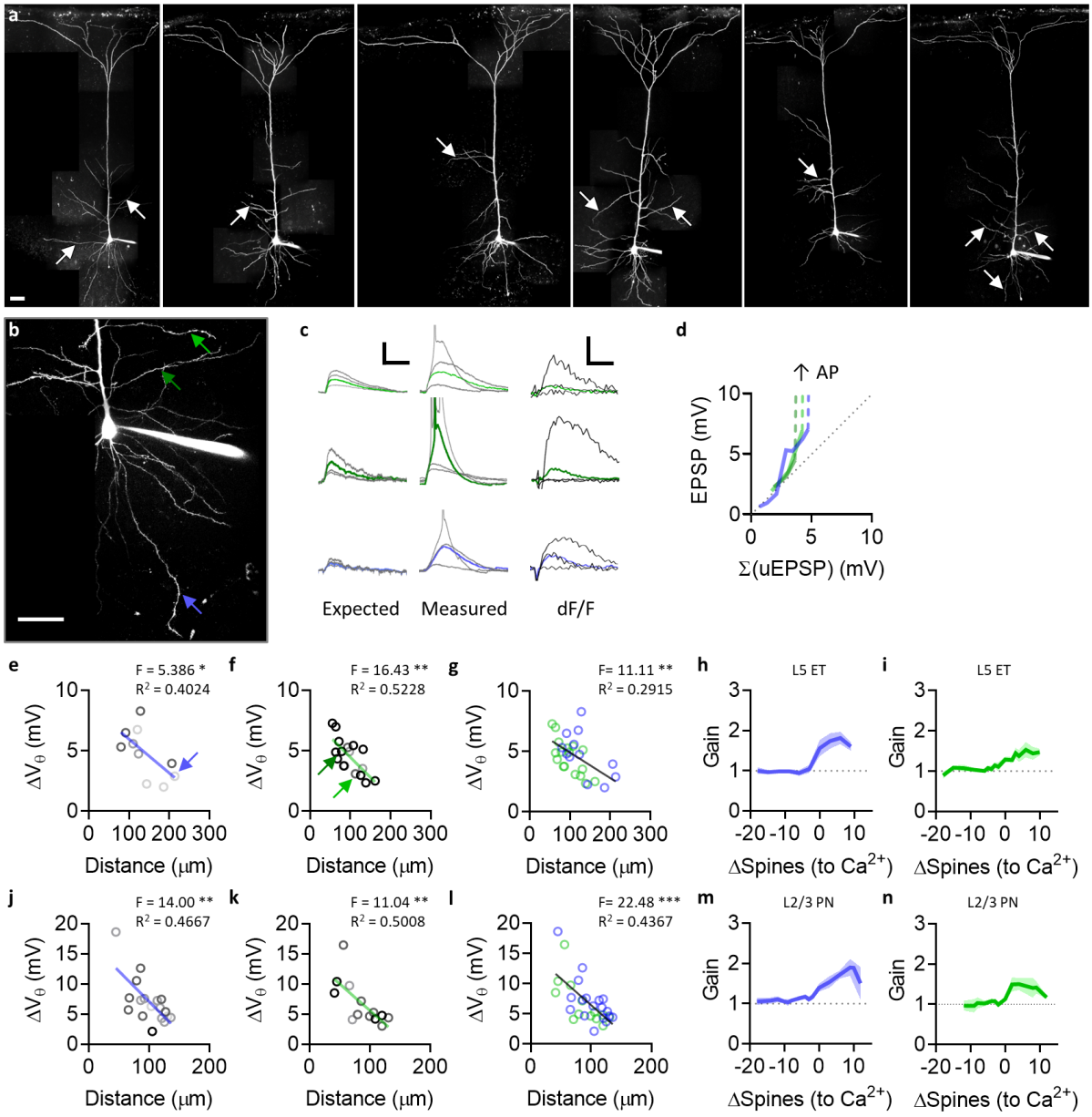
a
b
c
Expected
Measured
dF/F
d
↑ AP
EPSP (mV)
Σ(uEPSP) (mV)
e
F = 5.386 *
R² = 0.4024
f
F = 16.43 **
R² = 0.5228
g
F= 11.11 **
R² = 0.2915
h
L5 ET
i
L5 ET
ΔVθ (mV)
Distance (μm)
Gain
ΔSpines (to Ca2+)
j
F = 14.00 **
R² = 0.4667
k
F = 11.04 **
R² = 0.5008
l
F= 22.48 ***
R² = 0.4367
m
L2/3 PN
n
L2/3 PN

Figure 4. Somatic depolarization at nonlinearity threshold (ΔV_θ) is linearly correlated to synaptic distance from the nearest point on the apical trunk or the soma, in rodents as well as in humans, and for both supragranular and infragranular cortical pyramidal neurons. **(a)** Representative examples of rat L5 extratelencephalic (ET) PNs, from the temporal association area (TeA). Arrows indicate uncaging locations. Scale bar, 50 µm. Compare with **Fig. 1** for the difference in background caused by lipofuscin in the human cortex. **(b)** Representative example of a L5 ET PN, with three different uncaging locations; one on a basal dendrite, and two on separate oblique dendrites. **(c)** Representative traces from the uncaging locations shown in panel a. Scale bars, 50 ms, 5 mV, 0.5 dF/F. **(d)** Measured EPSP vs. expected EPSP from the sum of uEPSPs, from the branches shown in panels **b-c**. **(e-g)** ΔV_θ vs. synaptic distance as defined in **Fig. 2**, in rat L5 ET. **(e)** Basal dendrites. **(f)** Oblique dendrites. **(g)** Data shown in panels **e-f**, overlaid for comparison. **(h)** Synaptic gain, at basal dendrites shown in panel **e**. **(i)** Synaptic gain, at oblique dendrites shown in panel **f**. **(j-n)** Similar to panels **e-g**, but from rat L2/3 PNs instead of L5 ET. **(j)** Basal dendrites. **(k)** Oblique dendrites. **(l)** Data shown in panels **j-k**, overlaid for comparison. **(m)** Synaptic gain, at basal dendrites shown in panel **j**. **(n)** Synaptic gain, at oblique dendrites shown in panel **k**.

105 **Table 1**

ID	Age	Sex	Area	Hemi.	Medications (AED)	Diagnosis	n (cells/humans)
BA14	-	-	ATL	-	-	Epilepsy	6
BA27	-	-	TL	-	-	Epilepsy	6
BB05	22	M	FL	-	-	Epilepsy	1
BF30	34	F	TL	-	-	Epilepsy	1
BI30	-	-	TL	-	-	Epilepsy	3
BJ04	-	-	TL	-	-	Epilepsy	3
BJ06	-	-	FL	-	-	Epilepsy	1
BK02	55	M	ATL	R	Le	Tumor	10
BK05	32	M	TL	L	Cb, Le, O, T	Epilepsy	2
BK10	71	F	TL	R	-	Tumor	13
BK18	46	M	FL	L	Ce, O, Ph	Epilepsy	7
BL06	71	M	TL	R	-	Epilepsy	13
CC07	33	M	FL	R	B, Lc, Lo	Epilepsy	12
CC17	23	F	ATL	R	Cn, G, Lm, Le, Lo, T, Z	Epilepsy	43*
CC31	24	M	ATL	R	Lc, Le, O, T	Epilepsy	1
CG05	18	F	TL	R	Cb, G, Lm, Le, O, T	Epilepsy	6
CH15	57	F	TL	R	Le	Tumor	9
CH16	24	M	TL	R	E, G, Lm, Le, O, Pe	Epilepsy	16
CI08	30	M	TL	L	Lm, Le	Epilepsy	1
DA31	72	F	TL	R	-	Tumor	4
DB16	31	M	TL	R	-	Epilepsy	7
DC15	71	M	TL	R	-	Tumor	7
						(Tumor)	43/5
						(Epilepsy)	119/17
						(Total)	162/22

Abbreviations:
B, brivaracetam; Ce, cenobamate; Cb, clobazam; Cn, clonazepam; E, eslicarbazepine; G, gabapentin; Lc, lacosamide; Lm, lamotrigine; Le, levetiracetam; Lo, lorazepam; O, oxcarbazepine; Pe, perampanel; Ph, phenytoin; T, topiramate; Z, zonisamide; -, not available (not applicable or unknown). Note that only limited information was made available for a subset of cases (n = 21/7, from a total of 162/22 (cells/humans)).

* Recorded up to 120 h post-resection (typically 24 to 48 h)

106 **Table 1.** Patient and tissue information.

Methods

Brain slice preparation

For human brain slices, tissue resected from patients was immediately placed in an ice-cold solution at the operating theater. The cutting solution used for transport and slicing contained (in mM): 165 sucrose, 20 HEPES, 25 $NaHCO_3$, 2.5 KCl, 1.25 NaH_2PO_4, 20 D-glucose, 5 sodium ascorbate, 3 sodium pyruvate, 0.5 $CaCl_2$, 7 $MgCl_2$, pH adjusted to 7.3 with NaOH, 300-310 mOsm. All materials were obtained from Sigma-Aldrich unless otherwise specified. The tissue bottle was kept in a thermally insulated container filled with ice packs and transported from the operating room at Massachusetts General Hospital (MGH) or Brigham and Women's Hospital (BWH) to the laboratory at Massachusetts Institute of Technology (MIT) within 25 minutes. The tissue block was then placed in a vibratome (VT1200S, Leica) for slicing, orthogonal to the pia to preserve cortical layers and white matter in proper orientation. Acute brain slices (300 µm in thickness) were made and maintained at 36 °C for ≥ 1 h in the recovery solution containing (in mM): 90 NaCl, 20 HEPES, 25 $NaHCO_3$, 2.5 KCl, 1.25 NaH_2PO_4, 20 D-glucose, 5 sodium ascorbate, 3 sodium pyruvate, 1 $CaCl_2$, 4 $MgCl_2$, pH adjusted to 7.3 with NaOH, 300-310 mOsm. All solutions were continuously aerated with carbogen (95% O_2, 5% CO_2) throughout the course of experiments, including transport and slicing, and refreshed every 6-8 hours. Experiments were performed within a period of typically 24 or 48 hours following resection, with exception (see Table 1). For rodent brain slices, 12-to-13-week-old male and female rats (Charles River) were anesthetized with isoflurane prior to decapitation; the cutting solution contained (in mM): 225 sucrose, 25 $NaHCO_3$, 2.5 KCl, 1.25 NaH_2PO_4, 20 D-glucose, 0.5 $CaCl_2$, 7 $MgCl_2$, 300-310 mOsm, and slices were recovered in artificial cerebrospinal fluid (aCSF) identical to the recording solution. A subset of the slices prepared for the current study was donated to be used elsewhere (Vardalaki et al., 2023). All protocols were approved by the internal review board (IRB) or the institutional animal care and use committee (IACUC) of the respective institution.

Whole-cell patch clamp

All human and rodent brain slice experiments were conducted under identical conditions. Slices were placed in a recording chamber and visualized with Dodt gradient contrast microscopy (Examiner Z1, Zeiss), while being perfused with the recording aCSF at 1.6 mL/min using a peristaltic pump (Minipuls 3, Gilson). The recording solution contained (in mM): 125 NaCl, 25 $NaHCO_3$, 3 KCl, 1.25 NaH_2PO_4, 10 D-glucose, 1.2 $CaCl_2$, 1.2 $MgCl_2$, 300-310 mOsm, maintained at 36 °C with an inline heating system (TC344C & SH28, Warner). Whole-cell patch clamp recordings were made from the soma of pyramidal neurons (PN) in layer 2/3 (L2/3) of the human neocortex, or L2/3 and L5 of the rat temporal association area (TeA), using a MultiClamp 700B amplifier (Molecular Devices). Data were bessel filtered at the cutoff frequency of 10 kHz, acquired at a sampling rate of 20 kHz, digitized and recorded with Prairie View (Bruker), then analyzed with PVBS (https://github.com/flosfor/pvbs). Patch pipettes (2.5-4.0 MΩ) were pulled from borosilicate glass capillaries (PG52151-4, WPI) with a horizontal pipette puller (P-1000, Sutter),

and positioned using a set of micromanipulators (Junior, Luigs & Neumann). The internal solution contained (in mM): 130 K-gluconate, 4 KCl, 4 NaCl, 10 HEPES, 15 phosphocreatine-di(tris), 4 Mg-ATP, 0.3 Na_2-GTP, adjusted to pH 7.3 with KOH, leading to final [K^+] of ~136-138 mM, and 300-310 mOsm. Additionally, 0.05 mM Alexa Fluor 594 and 0.1 mM Oregon Green BAPTA-1 (Thermo Fisher) were added to the internal solution for structural and calcium imaging. Pipette capacitance (C_p) was fully compensated, typically ~13.5-14.5 pF. Series resistance (R_s) was continuously monitored throughout the course of recordings, and cells with Rs ≤ 20 MΩ and change of less than 15% were accepted. To measure the intrinsic neuronal membrane properties, cells were held in current clamp at 0 pA, and injected at the soma with square current steps (-250 to +1000 pA in 50 pA steps, duration 500 or 1000 ms), with bridge fully balanced. Input resistance (R_{in}) was calculated from the linear regression crossing the origin from all subthreshold membrane potential responses to step current input; for hyperpolarizing pulses, transient-state membrane potential responses were used to minimize the contribution of hyperpolarization-activated current (i_h) in calculating of R_{in}. Sag ratio was defined as the difference between the transient-state and the steady-state membrane potential responses to -250 pA somatic current injection divided by the former, in alignment with the definition of R_{in}. Transient-state responses were calculated as the peak of the response in either direction, whereas steady-state responses were calculated as the mean from the later 20% of the step duration. Resting membrane potential (RMP) was calculated as the mean of the membrane potential during the baseline period preceding the current steps, typically 500 ms. For action potential (AP) waveform analysis, the first AP generated at rheobase was used. AP threshold was defined as the membrane potential immediately preceding the point at which the derivative of the membrane potential with respect to time (dV/dt) first exceeded 10 (V/s); for this purpose, data were further processed with a 4^{th} order bessel filter at the cutoff frequency of 4 kHz for noise reduction. AP amplitude was calculated as the difference between the AP peak and AP threshold, and the time between the two points at half of this amplitude respectively from the depolarizing and the repolarizing phase was taken as AP half-width. Liquid junction potential was measured at ~11-12 mV, but was not corrected for in the values of membrane potential reported in the current study.

2-photon glutamate uncaging and calcium imaging

All experiments were conducted at the 2-photon core facility (46-6178) at the McGovern Institute for Brain Research (MIBR), MIT. 2-photon excitation fluorescence microscopy (2PEF) for simultaneous structural imaging, glutamate uncaging (2PGU), and calcium imaging was performed using two Ti:sapphire lasers (Mai Tai eHPDS, Spectra Physics), modulated and guided using a custom-built optical setup including electro-optic modulators (M350-80, Conoptics) and an 8x pulse splitter (https://flosfor.github.io/pulse_splitter.pdf). Optical elements in the excitation and emission pathways were obtained from Thorlabs, or Chroma in the case of optical filters, unless otherwise specified. Signals were acquired with two photomultiplier tubes (H7422-40, Hamamatsu), after wavelength separation. For structural and calcium imaging, cells were visualized with Alexa Fluor 594 and Oregon Green BAPTA-1 as described above, respectively with 880 nm or 920 nm 2-photon excitation. For calcium imaging, line scans (256 repetitions of ~10 µm lines, each with ~1 ms duration at 8.25 µs/pixel) were made across the dendritic branch, near

the center of the synaptic spine cluster activated with 2PGU. The region of interest (ROI) and the background for the fractional change in fluorescence (dF/F) were defined respectively as those points with signal intensities above the 2nd percentile or below the 50th percentile from structural imaging, with the ROI consisting of continuous points flanked by two segments each including part of the background, during the baseline period prior to 2PGU pulse delivery. For 2PGU, 5 mM MNI-caged-L-glutamate (Tocris) was dissolved in the recording aCSF (adjusted to 120 mM NaCl from 125 mM to compensate for osmolarity), and delivered with minimal pressure using a puffer pipette of pore diameter ~15-20 µm, positioned ~100 µm away from the synaptic spines. 2PGU was achieved with 720 nm 2-photon excitation, quasi-simultaneously at an interval of 0.12 ms between spines with a dual galvanometer scanner (Bruker), ~0.1 µm from the head of each dendritic spine, at an intensity producing somatic uEPSPs within a range of physiological kinetics and amplitudes, typically ~0.1-0.5 mV (typically between ~50-150 mW past the 63x objective (421480-9900-000, Zeiss) in terms of the optical power of the excitation laser, but measured with continuous full-field illumination instead of short, focalized pulses used for actual 2PGU experiments). A total of 20-35 spines, typically spanning ~30-40 µm along a continuous segment, were activated at a given dendritic branch.

Data analysis

Electrophysiology and calcium imaging data were analyzed and visualized using PVBS (https://github.com/flosfor/pvbs). Structural imaging data were processed using imageJ (https://imagej.net) with the MosaicJ plugin (http://bigwww.epfl.ch/thevenaz/mosaicj). Plots were made using custom codes written in MATLAB (Mathworks), and Prism (GraphPad). Statistical information was expressed as mean ± standard error of the mean (SEM), where n indicates the number of branches or cells, as applicable. The skewness and the excess kurtosis of distributions were denoted respectively by G_1 and κ; G_1 is the Fisher-Pearson standardized third moment coefficient, and $\kappa = \mu_4/\sigma^4 - 3$, where μ_4 is the fourth central moment and σ is the standard deviation. Statistical comparisons were made with the Mann-Whitney U test, unless otherwise specified. Spearman's rank correlation coefficient (ρ) was used to evaluate correlations. Linear regressions were calculated based on the least squares method, whose slopes (m) were compared using the F-test including their deviation from zero. Statistical significance was accepted when the associated P value was below 0.05 (* $P < 0.05$; ** $P < 0.01$; *** $P < 0.001$).

Acknowledgements

We thank the clinical and research coordination personnel at MGH and BWH for the availability of human brain tissue for research. This work was supported by the Y. Eva Tan Fellowship from the Yang-Tan Center for Molecular Therapeutics in Neuroscience at MIT (2021-2023, to J. Y.).